mathematics

MDPI

Article

Understanding In-Line Connections Behavior from Experimental and Numerical Analyses on Rectangular and Circular Hollow Section Elements

Calin-Ioan Birdean [1], Ioan Both [2,*], Ioan Mărginean [2] and Anghel Cernescu [1]

[1] Department of Mechanics and Strength of Materials, Politehnica University of Timisoara, 300222 Timisoara, Romania; calin.birdean@student.upt.ro (C.-I.B.); anghel.cernescu@upt.ro (A.C.)
[2] Department of Steel Structures and Structural Mechanics, Politehnica University of Timisoara, 300224 Timisoara, Romania; ioan.marginean@upt.ro
* Correspondence: ioan.both@upt.ro

Abstract: Depending on the connection type, especially semi-rigid connections, the analyses of building structures offer accurate results function of the rigidity and ductility. The present paper analyzes the in-line connection of rectangular and circular hollow sections, categorized as semi-rigid connections, suitable for an architectural design of invisible joints. For such connection the standards do not cover an explicit design method. Experimental bending tests were performed on rectangular and circular hollow sections having the end plate fixed inside the profile and bolted by four and one high-strength bolts, respectively. The joint separation represents a serviceability criterion which was monitored using digital image correlation technique. Based on experimental results, a numerical model was validated using the finite element method. After the validation of the numerical model based on the experimental results, a parametric investigation was conducted to study the influence of the access hole, the preload level, the end plate thickness, and the axial force. The results show the small influence of the bolt preload, but the end plate thickness was of major importance. A reduction of the assembly rigidity was also caused by the manhole. The study shows the feasibility of the connection configuration with the end plate positioned inside the hollow profile.

Keywords: in-line connection; experimental test; finite element analyses; joint separation; parametric study

MSC: 65Z05

Citation: Birdean, C.-I.; Both, I.; Mărginean, I.; Cernescu, A. Understanding In-Line Connections Behavior from Experimental and Numerical Analyses on Rectangular and Circular Hollow Section Elements. *Mathematics* **2023**, *11*, 3416. https://doi.org/10.3390/math11153416

Academic Editors: Joaquim Infante Barbosa and José Alberto Rodrigues

Received: 16 July 2023
Revised: 30 July 2023
Accepted: 3 August 2023
Published: 5 August 2023

1. Introduction

For an attractive aspect of steel structures, rectangular or circular hollow sections are welded leading to a continuous aspect of the structure. This solution involves specialized manpower and requires more time for erecting. Bolted connections provide sufficient capacity and rigidity if used for hollow sections with end plates extended outside of the profile perimeter as presented by [1]. By positioning the bolts only within the perimeter of the profile, the response of the connection is highly affected by lowering both the rigidity and the capacity. Nevertheless, the bolted connection has the advantage of a reduced erecting time compared to the welded connection.

In the case of T joints where distribution of moment is very important, the rigidity of welded joints for hollow sections reduces, if the axial force leads to stresses close to the yielding of material [2]. Similar studies were conducted to determine the bending capacity, rotational stiffness and ductility for high strength steel connection which proved the need for reduction coefficients only for few welding types [3].

When different profiles of tubular sections are connected by welding, the push–pull local mechanism is the common failure mode for which the rotational stiffness may be of

high importance. Design methods for T joints were suggested by Szlendak [4], but the in-line connection failure mode, which is the current interest, is very different as the web of the element is not an influencing factor.

For the continuity connection of tubular sections, end plates connected by bolts can be used. The thickness effect on the prying force for bolted flange connection with the bolts positioned outside the profile perimeter was shown by Liu et al. [5]. The study also presented flange thicknesses, bolt edge distances, flange edge widths, and bolt hole diameters influence, both experimentally as well as numerically.

For high levels of forces, inner and outer bolts can be used for the flange connection of hollow sections as presented by Li et al. [6]. This connection exhibits a more direct stress distribution.

Another improved connection was presented by Deng et al. [7], the external double-layered flange connection, which overcomes the brittle fracture and the lamellar tearing of traditional flange connections.

Such connections are highly used for steel antenna towers [8] either for unipole or truss configurations, and for modular steel constructions and the joints types presented in [9]. Among these connections, the hidden joints are of interest due to their aesthetic aspect. Due to the small distance between the compressed area and the tensioned bolt, the rigidity of such connections is limited, and the joint is considered a semi-rigid joint. For structures with semi-rigid joints, the real deformation of the structure is obtained only if the rigidity of the joints is considered. The influence of the axial and bending level on the rigidity of the semi-rigid joints was presented in [10].

Structures with hollow sections require supplementary strength for seismic design. An innovative dismountable joint based on container corner fitting is proposed by Lian et al. [11] and its seismic performance is investigated based on FE analysis. The study showed a simplified connection that substitutes the bolt modeling with multiple connectors.

The stability of square hollow sections in comparison to concrete-filled steel tubes used in the case of modular construction was presented by Chen et al. [12] for which the connections are also similar to the section dimensions. These connections usually use high-strength bolts, but a 20% lighter cast–steel connector can be used without compromising the strength needed to satisfy the design loads [13].

In a numerical study, Urbonas and Daniunas [14] showed that the inclination of the beam, and quantity and location of bolts have a significant influence on joint rigidity.

The aesthetic aspect of the element can be maintained using an end plate with the same perimeter as the hollow profile as presented by Both et al. [15], where the failure modes, both welding and bolt failure, were also highlighted after an experimental testing program on in-line connections of rectangular hollow sections. This configuration is susceptible to lamellar tearing [16]; thus, the current studied configuration eliminated this risk.

In addition, the prying forces developing in these connections represent a risk factor, and the force in the bolt can be calculated using the relations developed by [17]. The current configuration eliminates the development of the prying forces as the end plates are not in contact.

Based on the classical strain iteration algorithm for cross sections, in practice, the assessment of the capacity can be determined using the method developed by Stephan and Stutzki [18]. The method is suitable for computer programs but the magnitude of the joint separation in the tensioned area is not available, although it can be a serviceability criterion for design.

These in-line connections are mostly used for axial force transfer between the elements, but bending can also occur. Thus, the response of these joints to flexural loading is necessary to be studied either for the resistance or for the deformation.

The paper presents the response of an in-line bolted connection with the end plate positioned inside a rectangular or circular hollow section at 2 mm from the profile end plane, with access through a hand hole. Based on experimental results, a numerical model is defined using the finite element method. After the validation of the numerical model

based on the experimental results, a parametric investigation is conducted to study the influence of the access hole, the preload level, the end plate thickness, and the axial force.

2. Materials and Methods (Experimental Tests)

As the results of the numerical simulation are based on experimental results, the following relates to the testing data.

Two tests were performed on each rectangular hollow section (RHS) and circular hollow section (CHS) specimen subjected to bending. The length of the specimen was different resulting in the loading position and the boundary conditions presented in Figure 1. Both supports allowed free rotation while only one allowed horizontal displacements.

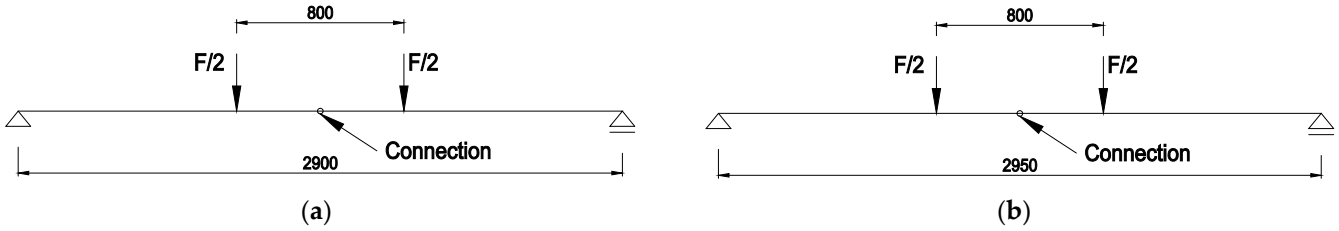

Figure 1. Static scheme for: (**a**) RHS; (**b**) CHS.

Each tested specimen implied two assemblies connected in the middle of the span. The rectangular specimens considered the RHS250 × 150 × 8 profile, with the details of the specimen presented in Figure 2.

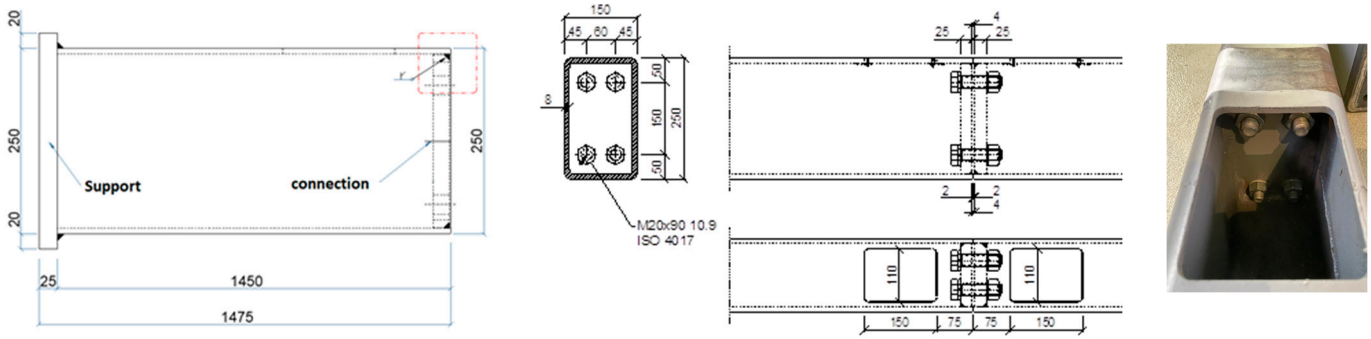

Figure 2. Details of RHS specimen.

The circular specimen considered the CHS114.3 × 10 profile, with the details of the specimen presented in Figure 3.

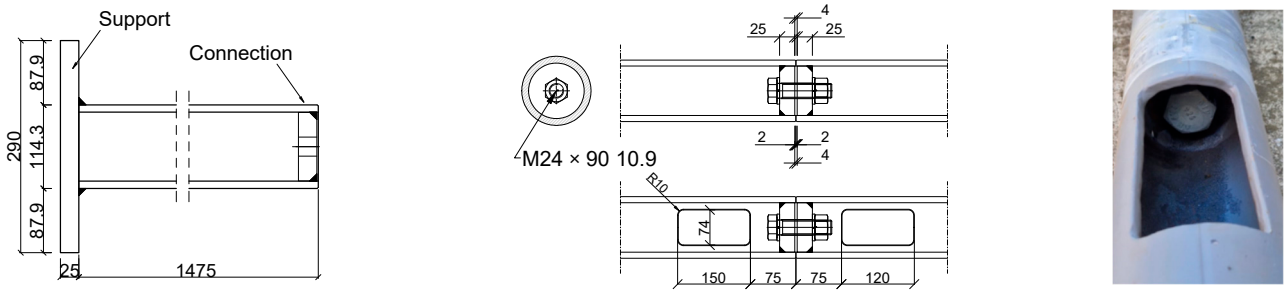

Figure 3. Details of CHS specimen.

Each element assembly had a cut of 150 mm long and a width of 110 mm and 74 mm for the RHS and CHS specimens, respectively. The RHS was connected using four M20 gr.

10.9 bolts, while the CHS was connected by one M24 gr. 10.9 bolt. The torque wrench was set to introduce a 130 kN preload force.

It must be mentioned that the end plates had a thickness of 25 mm and were inserted in the profiles at a distance of 2 mm from the profile end, to allow perfect contact between the hollow sections and avoid contact between the welding of the end plates.

The entire setup of the experimental tests is presented in Figure 4. A supplementary structure (yellow structure) was assembled to avoid out-of-plane displacements of the actuator and the specimens.

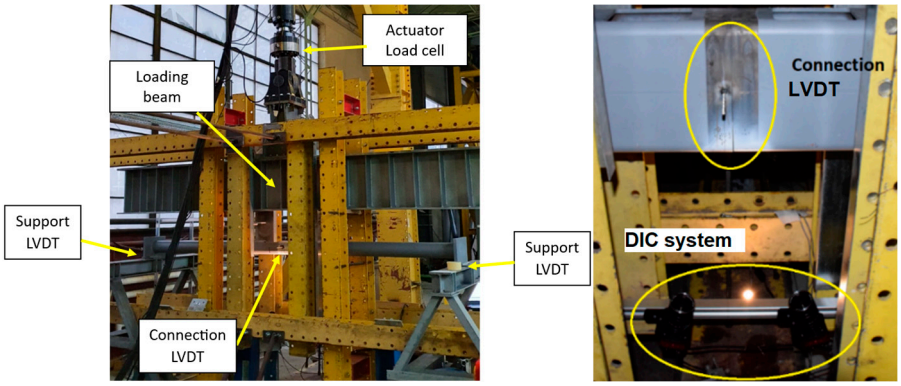

Figure 4. Test setup.

The recordings of the experimental tests consist of the vertical displacements at the supports and midspan, and the force obtained from the actuator. The vertical displacements were measured by linear variable displacement transducer (LVDT) while the force was measured by the actuator load cell.

The transmission of loading forces was achieved by means of devices that allowed the loading points to rotate freely. In the case of RHS profiles, the device contains a roller and parts to distribute the load over the entire width of the upper flange, Figure 5a, while for CHS profiles, a steel part was cut out to transmit the loads to the upper contour of the profile, Figure 5b.

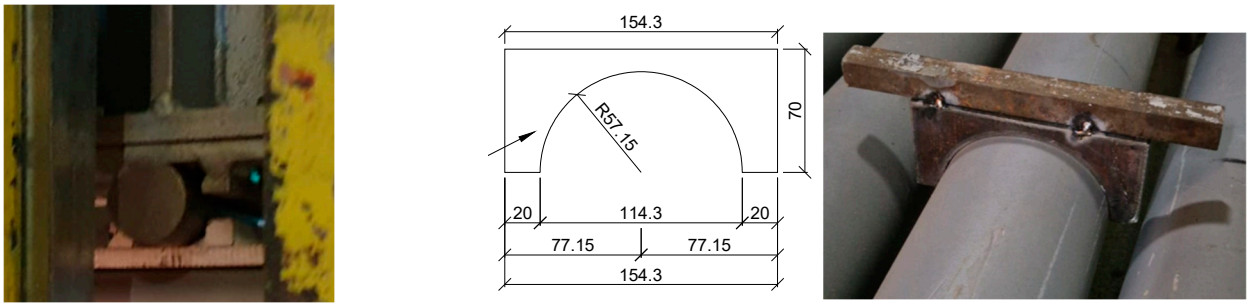

(**a**) (**b**)

Figure 5. Loading devices for: (**a**) RHS; (**b**) CHS.

The mechanical properties of the base material were determined according to ISO 6892-1 [19] on two specimens extracted from the specimen profiles as presented in Figure 6. Due to the available equipment, the specimens from the bolts were manufactured as presented in Figure 6c and they do not respect the proportionality factor.

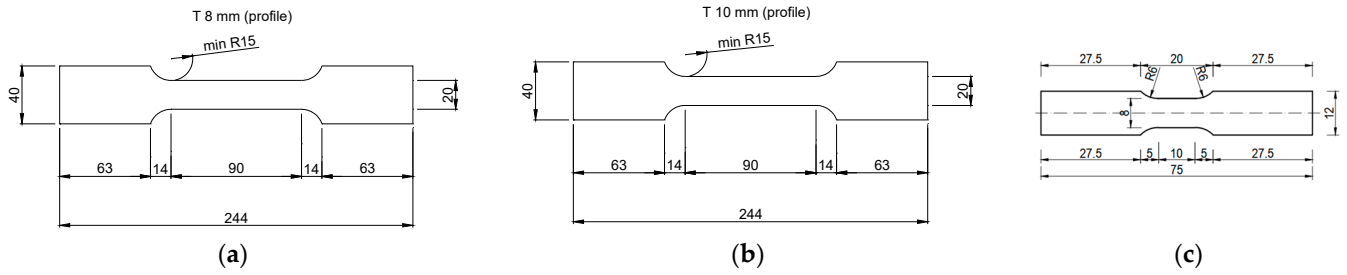

(**a**) (**b**) (**c**)

Figure 6. Tensile tests specimen for: (**a**) RHS; (**b**) CHS; (**c**) bolts.

The material characteristic curves are presented in Figure 7 where a small ductility is observed for the material of the CHS profile. Because the bolt tensile specimen is smaller than the standard specimen, the elongation of the material cannot be considered similar to the base material of the profiles.

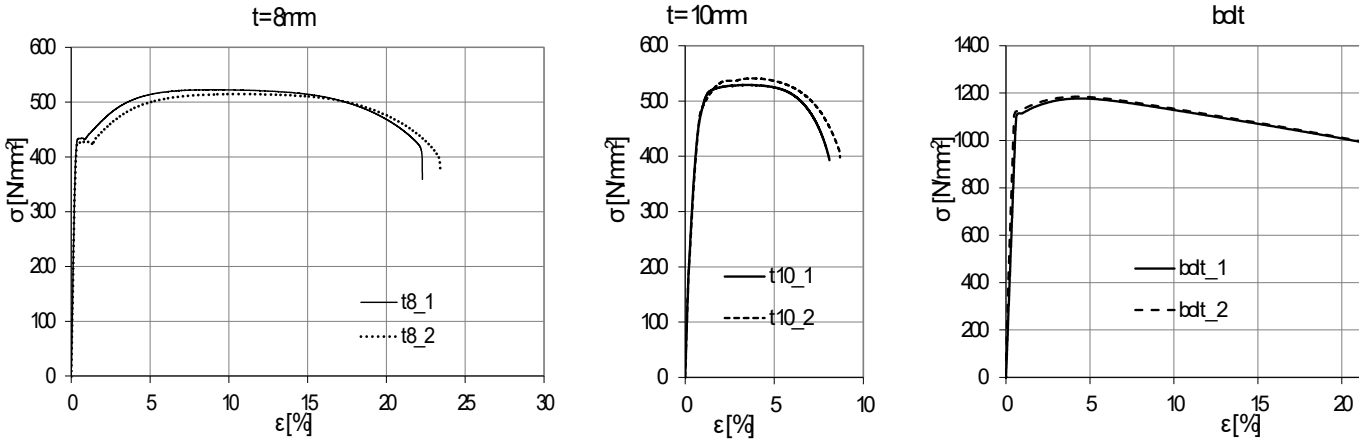

(**a**) (**b**) (**c**)

Figure 7. Base material characteristic curves for: (**a**) RHS; (**b**) CHS; (**c**) bolt.

A major necking was observed for the material of the RHS profile compared to the necking of the material of the CHS profile in Figure 8, which explains the small ductility of the CHS material in the characteristic curve.

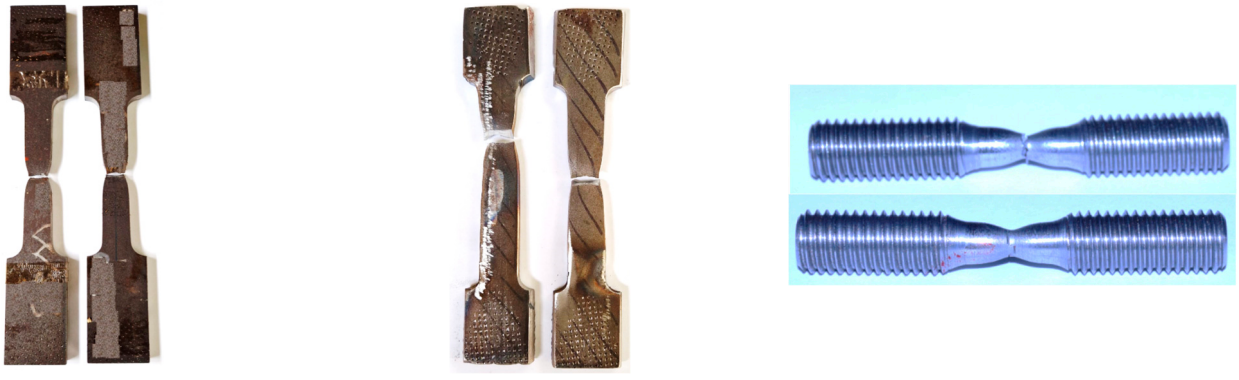

(**a**) (**b**) (**c**)

Figure 8. Fracture of the tensile specimens for: (**a**) RHS; (**b**) CHS; (**c**) bolt.

Based on the testing recordings, the following yield point and tensile strength were determined:

- 441–553 N/mm^2—RHS;

- 496–535 N/mm^2—CHS;
- 396–516 N/mm^2—end plate;
- 1119–1184 N/mm^2—bolt.

By transforming the characteristic curves into true stress-true strain, using the relations provided by Eurocode 1993-1-5 [20], the final value of the tensile strength used in the numerical model is 605, 564, 557, and 1231 N/mm^2, for the RHS, CHS, end plate and bolt, respectively.

The secondary interest of the experiments is the joint separation of the two hollow sections. Due to bolt pretensioning, the hollow sections should not separate immediately after loading. This parameter represents a serviceability limit state criterion. To monitor the joint separation, the digital image correlation (DIC) technique was employed with the system provided by isiSys GmbH. Black dots on a white background were applied on the tensioned side of each specimen to obtain the speckle pattern, Figure 9. Two virtual extensometers were defined by connecting two virtual gauges defined on each side of the connection.

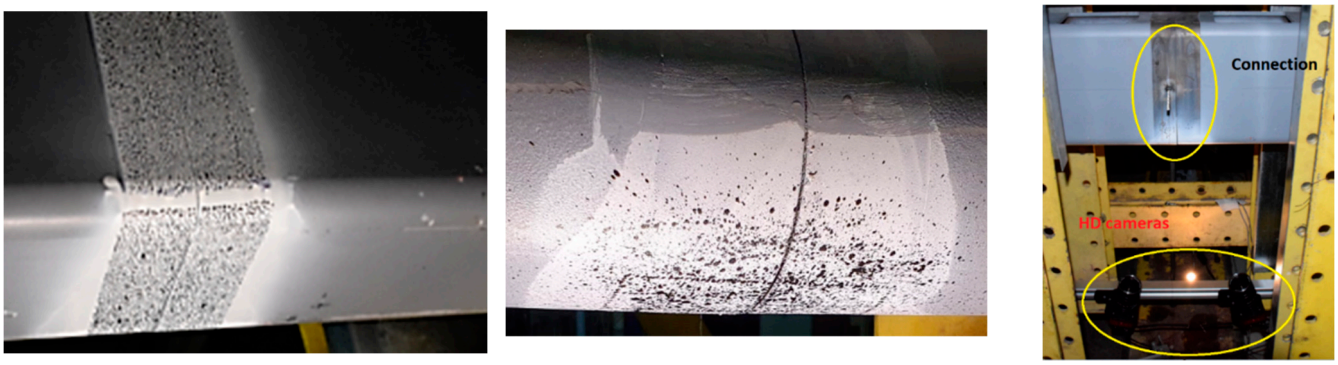

(**a**) (**b**) (**c**)

Figure 9. (**a**) Speckle pattern for RHS; (**b**) speckle pattern for CHS; (**c**) setup for the DIC system.

The DIC allows the displacement monitoring of the virtual gauges and the distance between them by using VIC Gauge 3D v7 software as well as the strain in the monitored area by using VIC 3D on the images captured by the high-resolution cameras.

3. Materials and Methods (Numerical Simulations)

The finite element analysis was conducted using Abaqus 2017 [21] software. The principle for using numerical analysis is to avoid expensive physical tests to evaluate the effect of different parameters. Numerical analyses can be performed in various formulations but the most effective is desired. An optimization has to be found between the precision and the complexity of the model. The current study simulates the connection between hollow sections which, from the experimental tests, was proven to reach the maximum capacity at bolt failure. Because stability phenomena are not influencing the response of the assembly, the standard static analysis is employed and, as it will be shown, will provide accurate results. Based on the validated model which provides similar results as the data recording during the experiment, the effect of the access hole, bolt preload, and end plate thickness is assessed.

Three-dimensional solid elements were defined as parts of the assembly similar to the entire experimental specimen (Figures 10 and 11 for RHS and CHS, respectively). The static, general solver was employed for the analysis during loading.

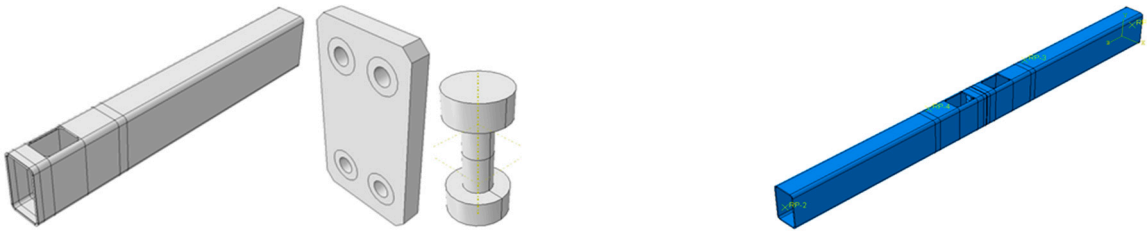

(**a**) (**b**)

Figure 10. Finite element model for RHS: (**a**) individual parts; (**b**) assembly.

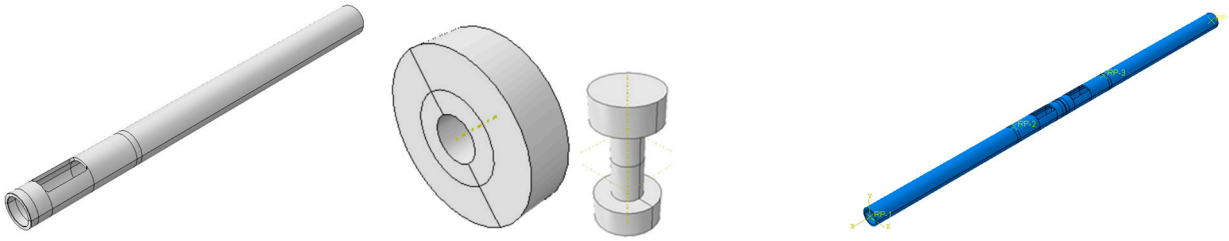

(**a**) (**b**)

Figure 11. Finite element model for CHS: (**a**) individual parts; (**b**) assembly.

The material properties considered an elasticity modulus of 210,000 N/mm^2 while the strength and deformation were defined with the true stress obtained from the tensile tests as presented in Table 1.

Table 1. Mechanical properties for the finite element model.

Material	Yield Stress $R_{p0.2}$ [N/mm^2]	True Tensile Strength R_m [N/mm^2]	Percentage Plastic Extension at Maximum Force A_g [%]
t = 8 (RHS)	441	605	8
t = 10 (CHS)	496	564	4
End plate	396	557	10
Bolt	1119	1231	5

The contact interaction was defined for normal and tangential behavior. The tangential contact defined with a *Penalty* friction formulation, with isotropic directionality, and a 0.1 friction coefficient. The theoretical relation for such contact is given in Abaqus Documentation [21] with an equivalent tangential stress being less than the critical tangential stress which is proportional to the contact pressure by the friction coefficient, see Equation (1). The stiff elastic behavior was modeled by the *stiff elastic behavior* for which the condition is not applied pointwise but weighted over a small area. This allowable maximum elastic slip is considered the default value of 0.5% of the average length of all contact elements [21].

$$\tau_{eq} = \sqrt{\tau_1^2 + \tau_2^2} < \mu \cdot p = \tau_{crit} \quad (1)$$

For the normal behavior, the *Hard* contact formulation was selected with the default direct method as a constraint enforcement method which attempts to strictly enforce a given pressure–overclosure behavior per constraint, without approximation or use of augmentation iterations. In addition, separation after contact was allowed.

The contact was defined as *surface-to-surface* interactions for the following pairs: bolt head and first end plate, bolt nut, and second end plate, hollow section ends in contact (Figure 12).

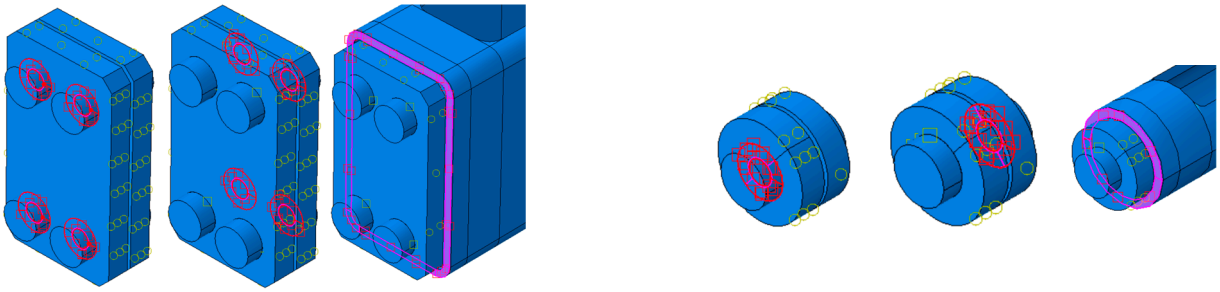

(**a**) (**b**)

Figure 12. Contact interactions: (**a**) RHS; (**b**) CHS.

A pinned and a roller support were defined at the assembly ends using a coupling constraint controlled by a reference point (Figure 13).

(**a**) (**b**)

Figure 13. Support conditions: (**a**) RHS; (**b**) CHS.

The loading areas are defined also in a kinematic coupling constraint controlled by reference points which have an imposed vertical displacement of 50 mm (Figure 14).

(**a**) (**b**)

Figure 14. Loading areas for: (**a**) RHS; (**b**) CHS.

The end plate was connected to the RHS or CHS profile using the Tie constraint. Supplementary, contact interactions are necessary to be defined between the bolts and the end plate, and between the two hollow profiles which are in contact.

The contact interaction was defined as normal and tangential behavior, allowing separation after contact. The tangential contact was defined with a 0.1 friction coefficient.

Each part was meshed with C3D8R (an 8-node linear brick, reduced integration, hourglass control) finite element type. The size of the element was approximately 5 mm, with smaller elements being defined for the bolts, allowing 2 elements on the thickness of the hollow element wall (Figure 15). In order to reduce the computation time, the length of the finite element in the longitudinal direction was increased.

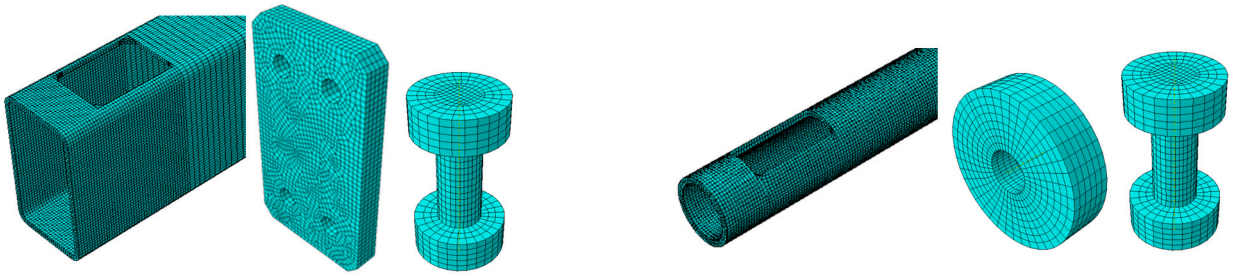

(**a**) (**b**)

Figure 15. FEM mesh for parts: (**a**) RHS; (**b**) CHS.

For the bolts, a preload of 130 kN was defined in a separate step before the applied load, analyzed in a static step. The preload propagation was modified to "Fix at current length" for the following analyzing steps, to allow the development of internal stress in the bolts due to bending of the specimen.

4. Results

4.1. Experimental Results

From the recordings of the experimental tests, Force-Displacement curves were obtained as presented in Figure 16. Of course, the capacity of the RHS is bigger than the capacity of the CHS as well as the rigidity. It must be mentioned that the observed failure mode for both sections was bolt failure but the RHS specimen showed a redundant behavior due to the number of bolts, while the CHS specimen had a brittle failure mode, after the shank fracture the entire assembly could not resist any force. The failure mode of the bolts used in the RHS connection is the thread stripping while for the CHS connection is the shank fracture, as presented in Figure 16.

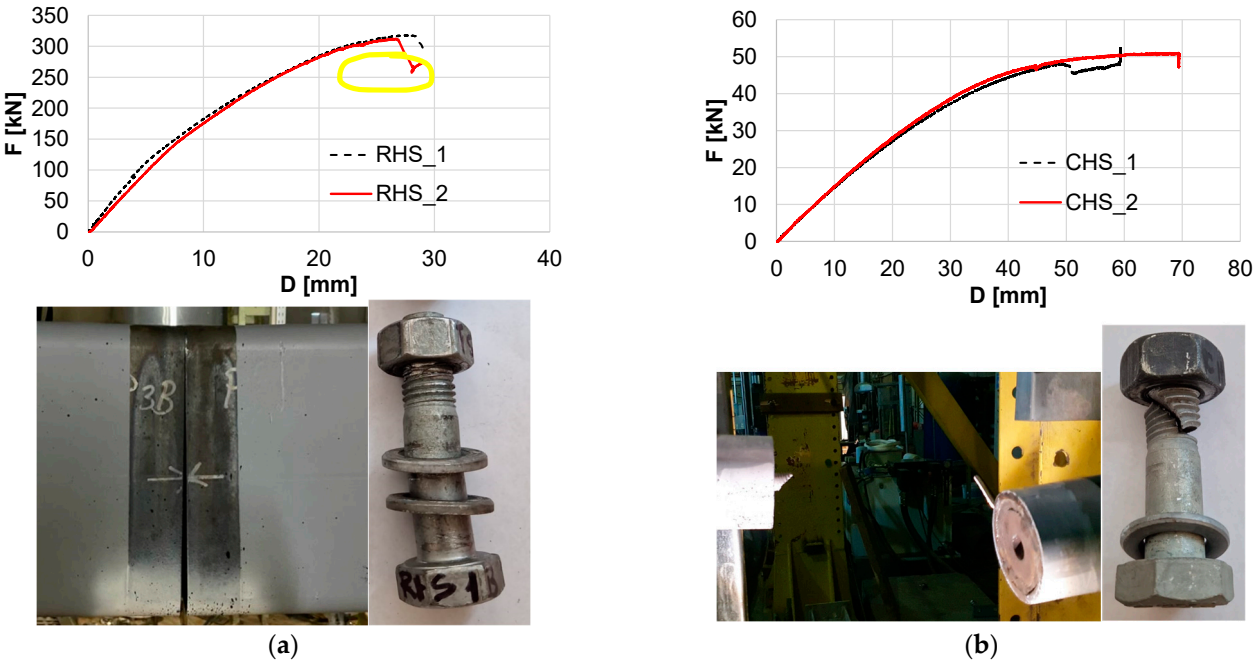

(**a**) (**b**)

Figure 16. Force displacement curves and failure modes: (**a**) RHS; (**b**) CHS.

The DIC results are presented in Figure 17. Comparing the two graphs, it is observed that the increased rigidity of the RHS maintains the profiles in contact for a significant amount of force, approximately 50% of the maximum force. On the other hand, the CHS connection starts to separate in the tensioned area from the initial stage of loading.

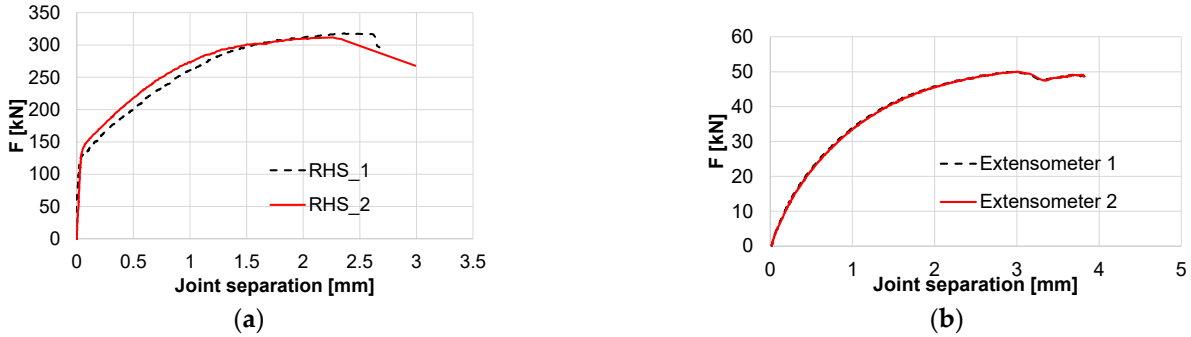

Figure 17. Joint separation recorded during experiments: (**a**) RHS; (**b**) CHS.

It must be mentioned that the separation is recorded after the pretensioning of the bolts which means that the initial compressive stress in the hollow profiles is not captured by the DIC system. Nevertheless, the compressive deformation of the profiles due to bolt pretension has a small value which can be determined by the numerical analysis.

4.2. Numerical Results

With the aforementioned parameters of the numerical model, the results of the finite element analysis are presented in Figure 18. The results of the numerical analysis follow in good accordance with the experimental results; thus, the model is considered to be validated for further studies.

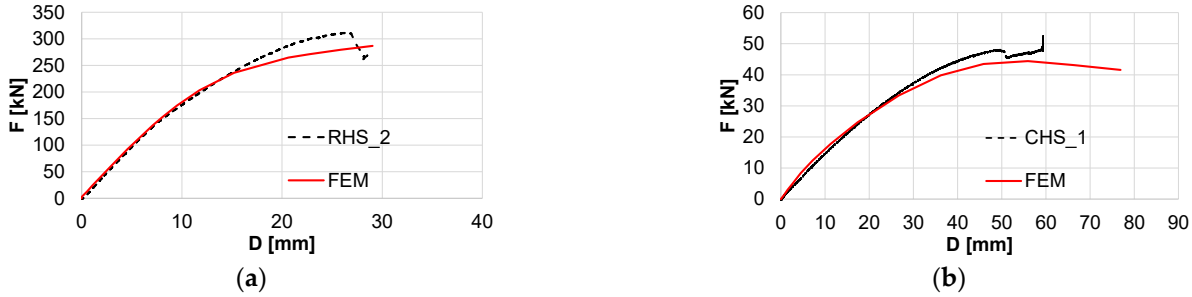

Figure 18. Experimental vs. FEM analysis: (**a**) RHS; (**b**) CHS.

The FEM model allows the assessment of stress distribution within the connection and furthermore, the bolts (Figure 19). Due to the flexibility of the end plate, a nonuniform distribution of the stress is observed on the profile contact for RHS, opposite to the CHS where the preload leads to a uniform pressure between the two profiles. Even in this stage, the bolts of the RHS connection are subjected to bending.

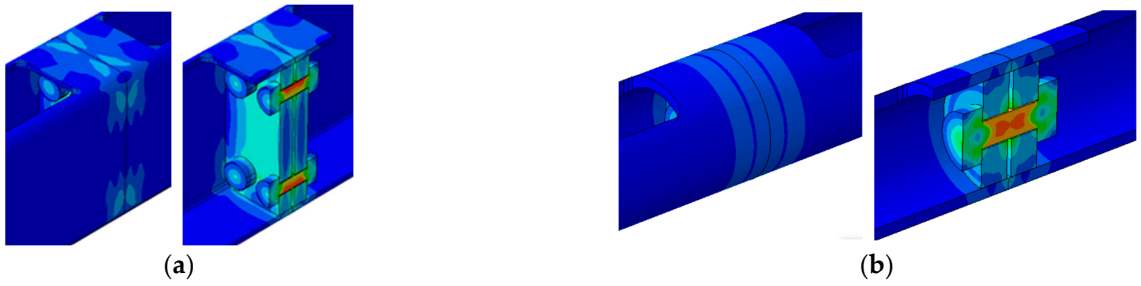

Figure 19. Stress caused by preload in the profile and in the bolts for: (**a**) RHS; (**b**) CHS.

By extracting the longitudinal displacements of the nodes close to the connection and adding the absolute value of the displacements of the two nodes, the joint separation was obtained (Figure 20). It must be mentioned that the preload introduced an initial

deformation of 0.045 mm and 0.004 for the RHS and CHS, respectively. These values were subtracted from the final joint separation as the deformations in the experiment were not included in the recordings of the DIC system.

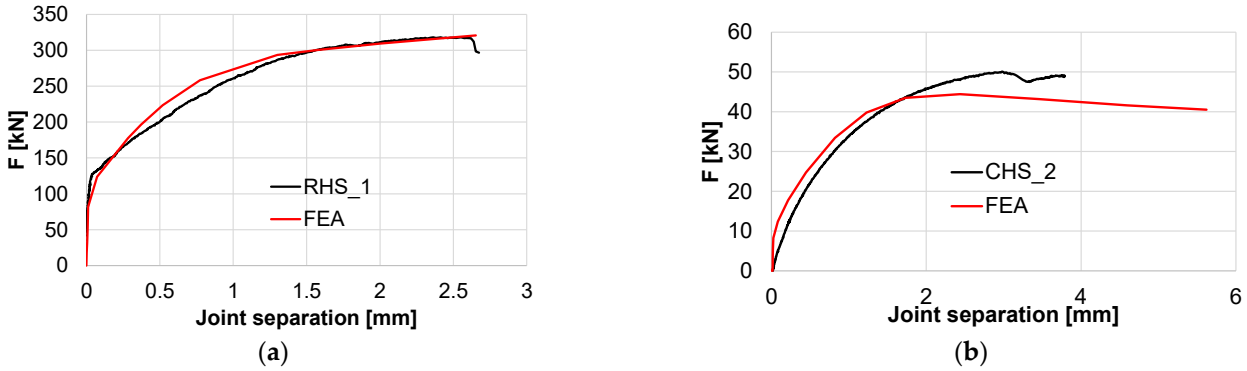

Figure 20. Joint separation: (**a**) RHS; (**b**) CHS.

For the RHS, the joint separation obtained by the FEA closely follows the recordings during the experiment, especially the first stage of the experiment where the two profiles are kept in contact. The CHS connection response obtained from the FEA is similar to the RHS analysis, showing an initial stage where the profiles are in contact, a phenomenon that was not observed in the experiment of CHS.

4.3. Parametric Study

4.3.1. Hand Hole Effect

A continuous hollow section was defined to study the influence of the hand-hole necessary for bolt assembling. This handhole is commonly covered by a plate connected by 2 small screws to plates welded to the interior of the hollow walls.

The results show an increased rigidity of the assembly but a similar maximum force for both RHS and CHS (Figure 21).

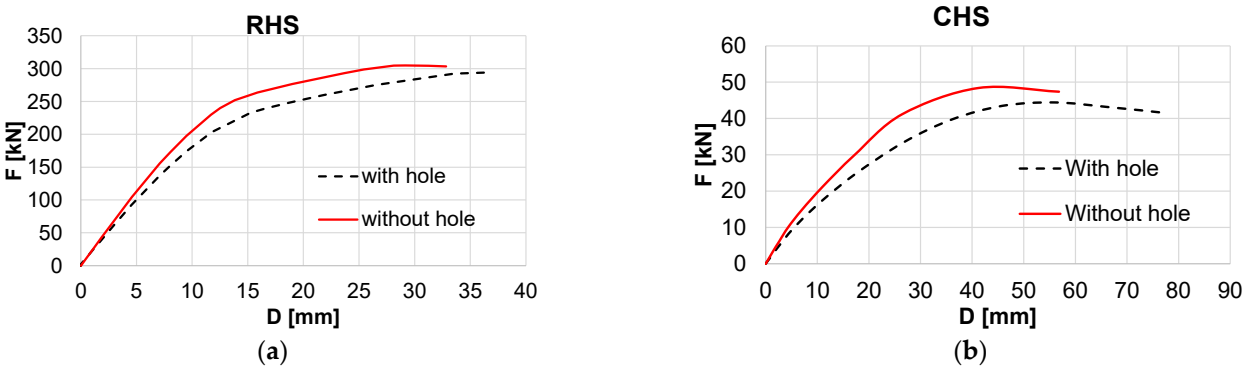

Figure 21. Hand hole effect: (**a**) RHS; (**b**) CHS.

4.3.2. Bolt Preload Effect

Bolt preload is required to have contact between profiles and perfect alignment at the time of assembling the structure. The RHS connection allows several bolts to be used while the CHS connections, which are usually of smaller sections, allow the use of one bolt. By considering different levels of preload, 0.3 ×, 0.5 ×, and 0.7 × Fy, where Fy is the nominal grade 10.9 yield force, the effect of the bolt preload was studied. A slightly significant increase of rigidity was observed for the RHS connection with the bolt preloaded at 200 kN, while for the other cases, the change of rigidity is neglectable, Figure 22.

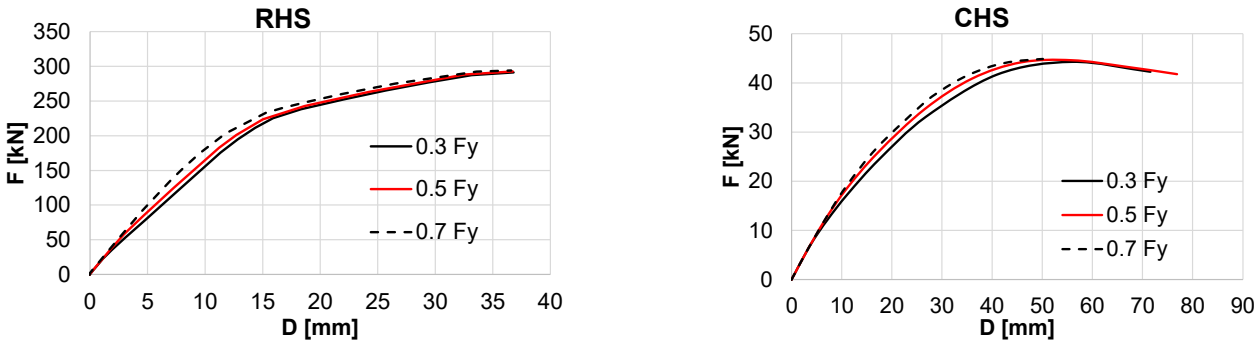

(**a**) (**b**)

Figure 22. Bolt preload effect on capacity: (**a**) RHS; (**b**) CHS.

Although the bolt preload effect on the capacity and the rigidity of the specimen is not significant, the joint separation, which is a serviceability criterion, is improved for the CHS connection, as depicted in Figure 23.

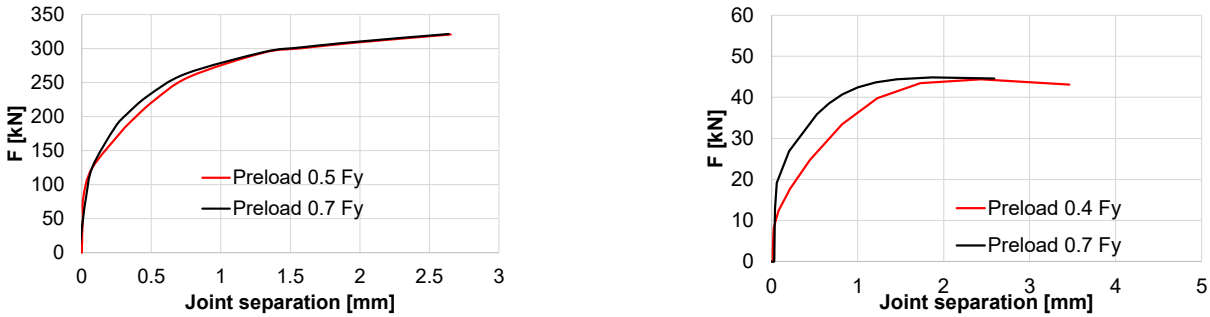

(**a**) (**b**)

Figure 23. Bolt preload effect on joint separation: (**a**) RHS; (**b**) CHS.

4.3.3. End Plate Thickness Effect

Although the two connections have different capacities, the end plate thicknesses considered for the parametric study were in the same range due to constructional reasons.

A significant loss of capacity is observed for the RHS connection although the initial rigidity is maintained at the same value. The CHS connection shows a 10% loss of capacity for similar plate thicknesses but for lower thicknesses the capacity reduces drastically, Figure 24.

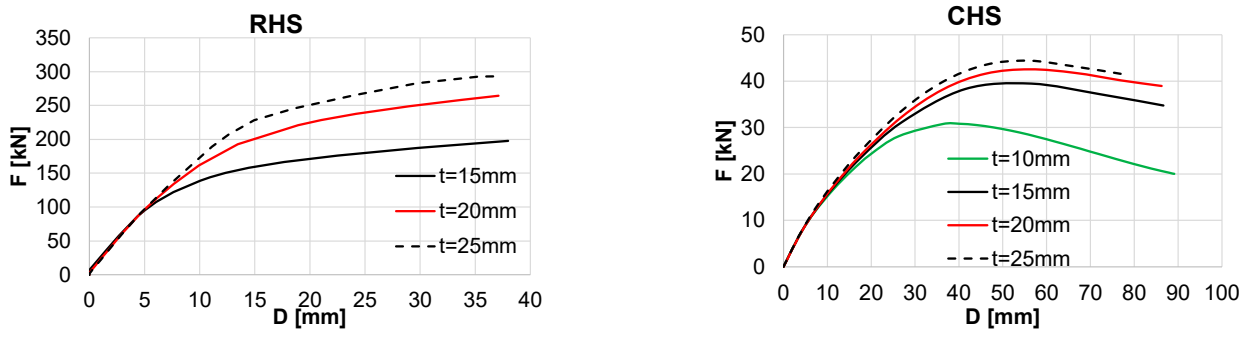

(**a**) (**b**)

Figure 24. End plate thickness effect: (**a**) RHS; (**b**) CHS.

Similarly, the rigidity of the connection starts to decrease after 50% of the maximum force. Due to the singular bolt of the CHS connection, the curve shows an increased softening with the smaller thickness.

5. Discussion

The current study intended to highlight the response, in terms of capacity and joint separation, and the failure mode of an in-line connection for rectangular and circular hollow sections with an end plate welded inside the tubular section. In such a configuration the bolted connection is not visible leading to an aesthetic visual effect. Similar studies were performed in the literature [15], with the end plate having external dimensions similar to the hollow section, resulting in a connection prone to welding failure.

Nevertheless, with a reduced lever arm of the bolts to resist the bending deformation of the joint, the capacity of the connection is limited. Experimental tests were conducted on two similar specimens for an RHS of 250 × 150 × 8 with an end plate of 25 mm and four bolts M20 gr. 10.9 and two specimens for a CHS of 114.3 × 10 with an end plate of 25 mm and one bolt M24 gr. 10.9. The two tests lead to similar results showing trustful results. By applying two symmetrical forces with respect to the connection, pure bending was the only internal force in the connection. The tested specimen was monitored by linear displacement transducers to obtain the midspan deflection while the force was monitored by the actuator loadcell. To record the joint separation, the digital image correlation technique was employed. Tensile tests were also performed to obtain the real mechanical properties of the base material of the RHS, CHS, and bolt.

From the experimental tests, the failure mode of the connection was observed in Figure 16. Both typologies failed by bolt fracture but the RHS, due to the multitude of bolts, experienced a safer collapse of the connection while the CHS profiles, connected by one bolt, completely detached from the connection. Force displacement curves were obtained from the acquisition system and joint separation was measured by the virtual extensometers of the DIC system.

The results of the experimental tests represent the basis of the numerical simulations performed by Abaqus [21]. As the failure mode of the specimens is bolt failure, static general analyses lead to satisfactory results if the preload force in the bolt was introduced. With the real material properties, the numerical analyses of the specimens showed good agreement with the experimental results both in terms of rigidity and capacity (Figure 18). By comparing the joint separation recorded by the DIC system to the FEM model, the RHS specimens also showed a good agreement, with minor separation until 35% of the maximum force, while, experimentally, the CHS connection started separating immediately after load application although numerically, the preload limited the separation until 20% of the maximum force applied.

The validated numerical models were then used for a parametric study considering: (i) the existence of an access hole for the bolt tightening, (ii) bolt preload, and (iii) end plate thickness.

A small increase of the capacity was observed for the specimens without the access hole, as the weak component was the bolt resistance, but a significant decrease in the deformation was observed especially for the CHS (Figure 21). Of course, the decreased rigidity due to an access hole was the proportion of the missing material in the position of maximum bending moment. For the maximum force applied, an increase of 9% resulted for the CHS while the RHS had a similar capacity.

For the three levels of preload, 0.3, 0.5, and 0.7 of the nominal yield force of the bolts used in the connection, M20 gr 10.9 and M24 gr 10.9, for the RHS and CHS, respectively, the flexibility of the end plate for RHS led to a neglectable influence on both rigidity and capacity of the connection, but the joint separation was reduced for the CHS, which has a more rigid end plate compared to the area of the cross-section of the hollow section (Figure 22).

The major influence on the connection response was represented by the end plate thickness. For flexible end plate 10 mm for CHS and 15 mm for RHS, the capacity was reduced by 34% and 32%, respectively. In the numerical simulation, although the contact was maintained for the first 20% of the maximum force, the joint separation was almost three times larger than for a rigid end plate (Figure 24).

The maximum forces obtained for different levels of preload and for the end plate thickness are summarized in Figure 25. The previously mentioned observations are observed in these graphs.

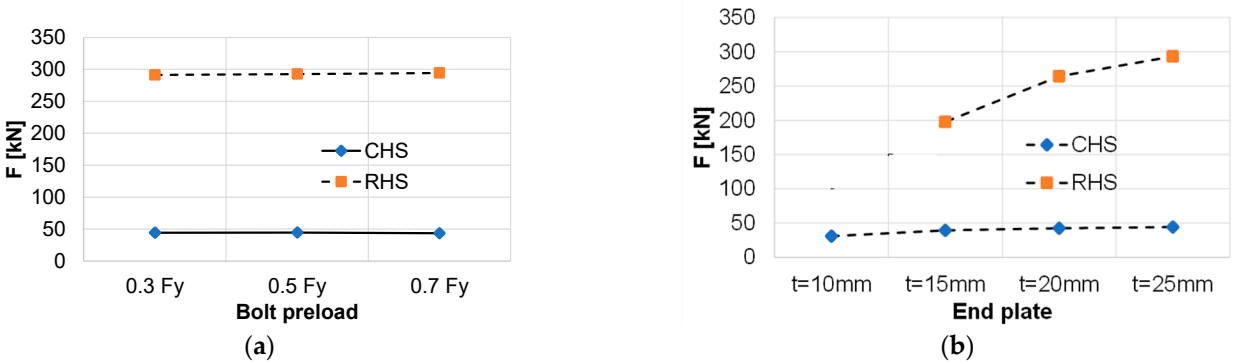

Figure 25. Maximum forces: (**a**) bolt preload; (**b**) end plate thickness.

The standards do not offer explicit design methods for these in-line connections although their use is becoming greater for aesthetic reasons. Based on the method presented by Stephan and Stutzki [18], the computer program GAS [22] allows the design of the connection but it does not offer any information about the joint separation. An estimation of the deformation in the joint can be related to the position of the neutral axis provided by the program. In Figure 26, the neutral axis for the RHS and CHS connections are presented considering the material properties obtained in the tensile tests and the preload of the bolts in the experiment. The defined bending moments to reach this position of the neutral axis were 41.5 and 5.25 kNm for the RHS and CHS, respectively. By determining the values of the bending moment according to Figure 1, the values corresponding to the inflection point in Figure 20 are 42.9 and 4.6 kNm. It can be seen that the values were very close; thus, the numerical model can predict the joint separation.

Figure 26. Position of neutral axis according to [18]: (**a**) RHS; (**b**) CHS.

Although the discussions were focused on RHS and CHS, it must be mentioned that the two typologies are related to the size of the elements. The small size of rectangular hollow sections can also be used with only one bolt for the connection, and large circular hollow sections can have several bolts connecting the end plate inserted in the hollow section.

6. Conclusions

Depending on the purpose of the structure, the response of the in-line connection of hollow sections can relate to capacity, rigidity, and/or joint separation. The current study presents a feasible configuration of the in-line connection for which a continuous

aspect of the connected elements can be obtained. Without a standardized design method, it is shown that a simple numerical model can predict the response of the connection as validated based on the experimental results and analytical formulation.

Depending on the size of the element one or several bolts can be used for the connection. The connections using one bolt are prone to catastrophic failure as the connection has no redundant links.

The parameters affecting the capacity and the rigidity of the connection are the end plate thickness while the access hole and the preload affect in a small amount only the rigidity.

The parameters affecting the joint separation are the preload, if the end plate is not flexible, and the end plate thickness. Without a great material expense, a rigid end plate can reduce the joint separation as well as a controlled preload of the bolt.

Either rectangular or circular hollow section, the size of the element dictates the connection configuration which in any case has a smaller capacity than a continuous element due to the bolted connection, or a smaller rigidity due to the access holes.

Author Contributions: Conceptualization, C.-I.B. and A.C.; data curation, C.-I.B. and I.B.; funding acquisition, C.-I.B.; investigation, C.-I.B., I.B. and I.M.; methodology, I.B. and I.M.; resources, A.C.; software, C.-I.B.; supervision, A.C.; validation, C.-I.B., I.B. and A.C.; writing—original draft, C.-I.B.; writing—review and editing, I.B., I.M. and A.C. All authors have read and agreed to the published version of the manuscript.

Funding: This paper was financially supported by the project "Network of excellence in applied research and innovation for doctoral and postdoctoral programs/InoHubDoc", a project co-funded by the European Social Fund financing agreement no. POCU/993/6/13/153437.

Data Availability Statement: Data unavailable.

Conflicts of Interest: The authors declare no conflict of interest.

References

1. Liu, X.C.; He, X.N.; Wang, H.X.; Yang, Z.W.; Pu, S.H.; Ailin, Z. Bending-shear performance of column-to-column bolted-flange connections in prefabricated multi-high-rise steel structures. *J. Constr. Steel Res.* **2018**, *145*, 28–48. [CrossRef]
2. Garifullin, M.; Pajunen, S.; Mela, K.; Heinisuo, M.; Havula, J. Initial in-plane rotational stiffness of welded RHS T joints with axial force in main member. *J. Constr. Steel Res.* **2017**, *139*, 353–362. [CrossRef]
3. Havula, J.; Garifullin, M.; Heinisuo, M.; Mela, K.; Pajunen, S. Moment-rotation behavior of welded tubular high strength steel T joint. *Eng. Struct.* **2018**, *172*, 523–537. [CrossRef]
4. Szlendak, J. Beam-column welded RHS connections. *Thin-Walled Struct.* **1991**, *12*, 63–80. [CrossRef]
5. Liu, X.C.; He, X.N.; Wang, H.X.; Zhang, A.L. Compression-bend-shearing performance of column-to-column bolted-flange connections in prefabricated multi-high-rise steel structures. *Eng. Struct.* **2018**, *160*, 439–460. [CrossRef]
6. Li, Q.; Xu, C.; Luo, Z.; Huang, F.; An, Y.; Zhang, D.; Liu, P. Experiment and design methodology of an IODR flange connection under bending load. *J. Constr. Steel Res.* **2023**, *201*, 107744. [CrossRef]
7. Deng, H.-Z.; Li, C.; Song, X.-Q.; Li, F.; Fu, P.-C. Tensile resistance and design model of an external double-layered flange connection. *J. Constr. Steel Res.* **2019**, *161*, 309–327. [CrossRef]
8. Radu, D.; Feier, A. Steel antenna towers—From designing to manufacturing optimization. *Mater. Sci. Eng.* **2018**, *399*, 012047. [CrossRef]
9. Nadeem, G.; Safiee, N.A.; Bakar, N.A.; Karim, I.A.; Nasir, N.A.M. Connection design in modular steel construction: A review. *Structures* **2021**, *33*, 3239–3256. [CrossRef]
10. Urbonas, K.; Daniūnas, A. Behaviour of semi-rigid steel beam-to-beam joints under bending and axial forces. *J. Constr. Steel Res.* **2006**, *62*, 1244–1249. [CrossRef]
11. Lian, J.-Y.; Deng, E.-F.; He, J.-M.; Cai, L.-M.; Gao, S.-C.; Zhou, J.-J. Numerical analysis on seismic performance of corner fitting connection in modular steel building. *Structures* **2021**, *33*, 1659–1676. [CrossRef]
12. Chen, Y.; Hou, C.; Peng, J. Stability study on tenon-connected SHS and CFST columns in modular construction. *Steel Compos. Struct.* **2019**, *30*, 185–199.
13. Dhanapal, J.; Ghaednia, H.; Das, S.; Velocci, J. Structural performance of state-of-the-art VectorBloc modular connector under axial loads. *Eng. Struct.* **2019**, *183*, 496–509. [CrossRef]
14. Urbonas, K.; Daniūnas, A. Numerical tests of steel beam-to-column semi-rigid connections. *J. Civ. Eng. Manag.* **2003**, *9*, 292–296. [CrossRef]

15. Both, I.; Nunes, D.L.; Ivan, A.; Vucicevic, D. The Response of In-Line Connection of RHS Sections Subjected to Bending and Shear. In *Modern Technologies for the 3rd Millennium*; Nistor, S., Popoviciu, G.A., Eds.; Editografica S R L: Bologna, Italy, 2019; pp. 117–122. Available online: https://www.webofscience.com/wos/woscc/full-record/WOS:000617030100020 (accessed on 5 November 2022).
16. Feier, A.; Chivu, O.R. Lamellar tearing observations regarding the applications of European standards in the field of welded steel constructions. *Rev. De Chim.* **2018**, *69*, 352–1354. [CrossRef]
17. Huang, F.; Zhang, D.; Hong, W.; Li, B. Mechanism and calculation theory of prying force for flexible flange connection. *J. Constr. Steel Res.* **2017**, *132*, 97–107. [CrossRef]
18. Stephan, S.; Stutzki, C. A General Method for the Design of Bolted Connections for Space Frames. In Proceedings of the Fifth International Conference on Space Structures, Guildford, UK, 29 August 2002.
19. *EN ISO 6892-1*; Metallic Materials—Tensile Testing. Part 1: Method of Test at Room Temperature. CEN: Brussels, Belgium, 2009.
20. *EN 1993-1-5*; Eurocode 3: Design of Steel Structures—Part 1–5: Plated Structural Elements. CEN: Brussels, Belgium, 2006.
21. *Dassault Systemes, Abaqus 6.14 Documentation*; Simulia Systems: Providence, RI, USA, 2014.
22. *Gartner Steel and Glass*; Josef Gartner GmbH: Bayern, Germany, 2023.